Miren Isasa et al 2015 J. Phys. D: Appl. Phys. 48 215003

Spin transport enhancement by controlling the Ag growth in lateral spin valves

Miren Isasa[1,*], Estitxu Villamor[1], Lorenzo Fallarino[1], Olatz Idigoras[1], Anna K. Suszka[1,2], Christopher Tollan[1], Andreas Berger[1], Luis E. Hueso[1,3] and Fèlix Casanova[1,3]

[1]CIC nanoGUNE, 20018 Donostia-San Sebastian, Basque Country, Spain.
[2]current address: Laboratory for Mesoscopic Systems, Department of Materials, ETH Zurich, 8093 Zurich, Switzerland, Laboratory for Micro- and Nanotechnology, Paul Scherrer Institute, 5232 Villigen PSI, Switzerland.
[3]IKERBASQUE, Basque Foundation for Science, 48011 Bilbao, Basque Country, Spain.

*E-mail: m.isasa@nanogune.eu

Abstract

The role of the growth conditions onto the spin transport properties of silver (Ag) have been studied by using lateral spin valve structures. By changing the deposition conditions of Ag from polycrystalline to epitaxial growth, we have observed a considerable enhancement of the spin diffusion length, from $\lambda_{Ag} = 449 \pm 30$ to 823 ± 59 nm. This enhancement in the spin diffusion length is closely related to the grain size of the Ag channel, which is 19 ± 6 nm for polycrystalline Ag and 41 ± 4 nm for epitaxial Ag. This study shows that diminishing the grain boundary contribution to the spin relaxation mechanism is an effective way to improve the spin diffusion length in metallic nanostructures.

A new generation of *spintronic* devices, which rely only on the electron spin degree of freedom, are envisioned for a future integration of logic and memory [1]. Creation, transport and detection of a pure spin current, *i.e.*, a flow of spin angular momentum without being accompanied by a charge current, are thus essential ingredients for a successful device. Lateral spin valves (LSVs) are basic *spintronic* devices that offer an attractive means to study the spin transport as well as the spin injection properties in different materials. After the pioneering studies, first by Johnson and Silsbee [2,3] and more recently by Jedema *et al.* [4,5], a large number of spin injection experiments have been reported in metals [6-23], semiconductors [24-26] or carbon-based materials [27,28]. LSVs consist of two ferromagnetic (FM) electrodes, used to inject and detect pure spin currents, bridged by a non-magnetic (NM) channel, which transports the injected spin current (see Fig. 1(a)). For the optimum performance of a LSV, it is crucial to choose a NM material in which the spin information can travel over long distances, *i.e.* with long spin diffusion length λ_{NM}, with Cu [4-12], Al [2,5,9,13,14] or Ag [15-22] being the most commonly selected metals. In order to enhance λ_{NM}, it is crucial to understand which are the spin relaxation processes that lead to the loss of spin information. It is known that, in NM metals, the spin relaxation is governed by the Elliott-Yafet (EY) mechanism [29,30], with phonons, grain boundaries, impurities or the surface being common sources for the associated spin-flip scattering [5,7,12,18,19]. A proper control of these contributions could thus help obtaining larger λ_{NM} values.

In this work, we explore a way of diminishing the grain boundary contribution to the spin relaxation by controlling the growth conditions of Ag. For this purpose, we have fabricated $Ni_{80}Fe_{20}$ (permalloy, Py)/Ag LSVs using an alternative fabrication process where the Ag channel is epitaxially grown. The epitaxial growth ensures that Ag grains will be well aligned, reducing the grain misalignment and enhancing transport phenomena. From non-local measurements we determine the spin transport properties of this epitaxial Ag channel, which are superior to those from polycrystalline Ag, which we also prepared as reference channel structures.

The fabrication of LSVs involves two metallization processes, one for the FM and the other for the NM metal. There are two common techniques for the fabrication process, namely: (i) a two-step electron-beam lithography (eBL) followed by metal deposition and lift off [4,6,16] and (ii) a two-angle shadow evaporation technique, where a single eBL step is required [8,9,13]. The only difference between them is that the two-step eBL process needs an extra milling step to obtain a clean FM/NM interface. In this article, we will use the eBL technique, for which the Ag channel will be defined in the first step and the FM electrodes will be patterned afterwards.

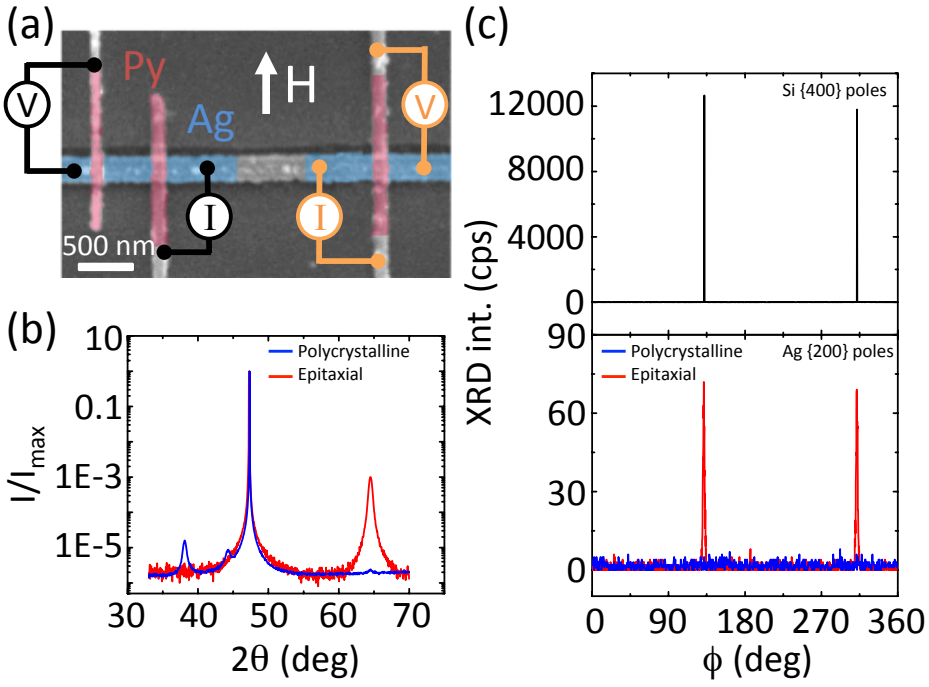

Figure 1. (a) Colored scanning electron microscope (SEM) image of a Py/Ag LSV, consisting of vertical Py bars on top of a horizontal Ag bar, and which was used to measure the interface resistance of Py/Ag. The FM and NM materials, the applied magnetic field (H) direction and the non-local (black) and interface resistance (orange) measurement configurations are schematically depicted. (b) XRD θ-2θ scan for epitaxial Ag (red line) and polycrystalline Ag (blue line). In the epitaxial case, the characteristic peak of Si (220) appears at $2\theta \simeq 47.30°$ and the peak of epitaxial Ag (220) appears at $2\theta \simeq 64.45°$. In the polycrystalline case, the characteristic peak of Si (220) appears at $2\theta \simeq 47.30°$ and the peaks of Ag (111), Ag (200) and Ag (220) appear at $2\theta \simeq 38.1°$, $2\theta \simeq 44.2°$ and $2\theta \simeq 64.45°$, respectively. Note that the Ag (220) peak in the polycrystalline case is not as pronounced as in the epitaxial case. (c) XRD ϕ-scans at the

2θ poles of the (100) planes of the Si substrate (top panel) and Ag thin films (bottom panel) for the epitaxial (red line) and polycrystalline (blue line) cases.

Thin films with 40 nm of epitaxial Ag were grown at room temperature by sputtering on a (110) Si substrate, after first removing the native Si-oxide by etching the Si-substrate with hydrofluoric (HF) acid [31,32]. For comparison, a control sample was fabricated following the same process, except that Ag was deposited without pretreating the Si substrate with HF acid, thus leaving the native oxide and leading to a polycrystalline Ag channel structure [33]. The structural analysis of the Ag films was performed via X-ray diffraction (XRD) measurements, utilizing a PANalytical X'Pert Pro diffractometer with Cu-K_α radiation. The crystal structure was checked by coplanar θ-2θ XRD measurements and ϕ scans (Figs. 1(b, c)). For the case of epitaxial Ag, from the θ-2θ scans only one diffraction peak at $2\theta \simeq 64.45°$, corresponding to the Ag (220) atomic planes, was observed together with the (220) Si substrate diffraction (Fig. 1(b), red line). On the contrary, for the polycrystalline Ag case (Fig. 1(b), blue line), three different diffractions peaks were measured, being $2\theta \simeq 38.10°$, which corresponds to Ag (111) atomic planes, the most pronounced peak. The in-plane orientation relationship between Si substrates and Ag thin films were investigated by means of XRD ϕ-scans at the {400} poles for Si and at the {200} for Ag. These ϕ scans clearly confirmed the epitaxial growth of Ag onto HF etched Si. As it can be clearly seen in Fig. 1c, both the Ag (red line, bottom panel) and the Si substrate (black line, top panel) show two diffraction peaks, corresponding to the two {100} poles, which are 180º apart and appear at the same absolute ϕ positions [34]. Regarding the ϕ scans (Fig. 1(c)) for the polycrystalline Ag (Fig. 1(c), blue line) only a more or less uniform background signal can be measured, as expected from a non-epitaxial structure. Furthermore, the average grain size for each sample can be extracted from the diffraction peaks by applying the Scherrer equation. From the (220) diffraction peak of the epitaxial Ag (Fig. 1(b)), a grain size of 41 ± 4 nm is obtained. On the other hand, using the same equation for the diffraction peaks of polycrystalline Ag, grain sizes of 15 ± 1 nm, 16 ± 2 nm and 26 ± 3 nm are obtained from the (111), (200) and (220) peaks, respectively, yielding an average value of 19 ± 6 nm.

After the structural characterization, the Ag films were coated with negative resist and, in an initial eBL step, a ~200-nm-wide channel was patterned. Ag was removed with two consecutive Ar-ion etchings (Fig. 2(a)). In the first etching, Ar ions were accelerated almost perpendicularly (80º from in-plane orientation) to the Ag surface in order to remove the Ag that was not protected by the negative resist. In this first step, some etched Ag was redeposited at the edges of the channel, forming vertical walls of Ag that needed to be removed. Therefore, a second etching was performed without breaking the vacuum by accelerating Ar ions almost perpendicular to these Ag walls (10º from in-plane orientation). The suppression of the redeposited metal was confirmed by observing cross-sectional cuts, produced by means of focused ion beam (FIB) irradiation after the first (Fig. 2(b)) and the second etching (Fig. 2(c)). After these etching processes, the samples were immersed in acetone, so that all the resist was removed. In a second eBL step, the FM electrodes were patterned using a positive resist in this case. 45-nm-thick Py was e-beam evaporated at a pressure of $\leq 1\times10^{-8}$ mbar and the samples were immersed in acetone for lift-off. Different Py electrode widths, ~110 nm and ~150 nm, were chosen

in order to obtain different magnetic switching fields. Each sample contains several LSVs where the edge-to-edge distance L between the Py electrodes varied between 150 and 5500 nm.

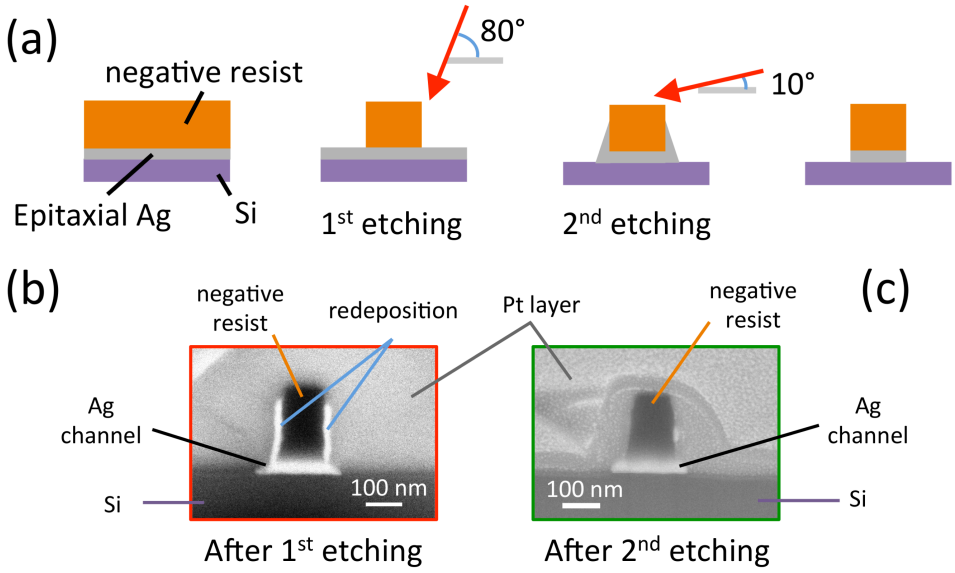

Figure 2. (a) Schematic representation of the two-step Ag milling. (b) Cross-sectional SEM image of the Ag channel just after the first etching. The vertical walls are redeposited Ag. (c) Cross-sectional SEM image of the Ag channel after the second etching. Vertical walls have been milled and the Ag channel has acquired the desired shape. Before cutting the cross sections by FIB, an initial e-beam induced deposition of Pt followed by ion-beam induced deposition of Pt was placed on top of Ag to protect the nanostructure, this is evident in the SEM images.

All measurements described in the following were carried out in a liquid-He cryostat (applying an external magnetic field H and varying the temperature T) using a "DC reversal" technique [9]. When a spin-polarized charge current is injected through the Py electrode, due to the net spin polarization of FM materials, a spin accumulation will be created at the Py/Ag interface and will diffuse to both sides of the Ag channel. The second Py electrode will detect the spin accumulation by measuring the voltage between the Py detector and the Ag channel. The measured voltage, V, normalized to the injected current, I, is defined as the non-local resistance $R_{NL} = \frac{V}{I}$ (See Fig. 1(a) for the measurement scheme). R_{NL} changes sign from positive to negative when the magnetization of the electrodes switches from parallel to antiparallel. We will call this change in resistance the spin signal ΔR_{NL} (Fig. 3(a)). As ΔR_{NL} is proportional to the spin accumulation at the detector, ΔR_{NL} will decay upon increasing the distance L at which the spin signal is detected (Fig 3(b)). Solving the corresponding one-dimensional spin-diffusion equation, the following expression is obtained for ΔR_{NL} [15,35]:

$$\Delta R_{NL} = \frac{4\,R_{Ag}\left[\alpha_i\left(\frac{R_i}{R_{Ag}}\right)+\alpha_{Py}\left(\frac{R_{Py}}{R_{Ag}}\right)\right]^2 e^{-L/\lambda_{Ag}}}{\left[1+2\left(\frac{R_i}{R_{Ag}}\right)+2\left(\frac{R_{Py}}{R_{Ag}}\right)\right]^2 - e^{-2L/\lambda_{Ag}}} \quad (1)$$

where R_i is the interface resistance, $R_{Ag} = \lambda_{Ag}\rho_{Ag}/w_{Ag}\,t_{Ag}$ and $R_{Py} = \lambda_{Py}\rho_{Py}/(1-\alpha_{Py}^2)w_{Ag}\,w_{Py}$ are the spin resistances, $\lambda_{Ag,Py}$ are the spin diffusion lengths, $\rho_{Ag,Py}$ are the resistivities and $w_{Ag,Py}$ and t_{Ag} are the geometrical parameters (width and thickness) of Ag and Py, respectively. α_{Py} and α_i are the spin polarizations of the Py and the interface, respectively.

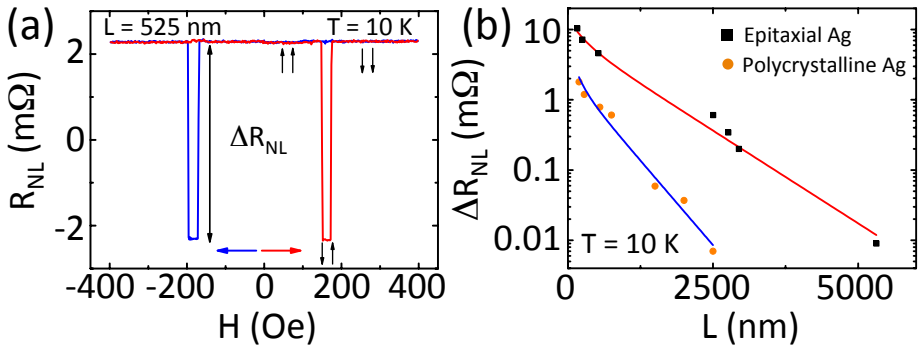

Figure 3. (a) Non-local resistance as a function of the applied magnetic field H at 10 K for a Py/Ag LSV with epitaxial Ag where L=525 nm. The spin signal is tagged as ΔR_{NL}. (b) Spin signal as a function of the distance L between the electrodes at 10 K in Py/Ag LSVs. The solid black (orange) squares (circles) are the experimental data for epitaxial (polycrystalline) Ag and the red (blue) solid line is the fit to Eq. (1).

A R_i of 60 mΩ is measured in the same device, in which the spin signal is obtained by using a cross-configuration that suppresses the contribution of the contacts, as shown Fig. 1(a). This measured value is in agreement with a non-transparent interface present in Py/Ag as previously observed [16,20,22]. The resistivity of Ag is measured using a 4-point configuration, in which a current is sent through the Ag channel and a voltage is measured using the Py electrodes. Varying the distance L in between the electrodes, the resistance of Ag for every L is measured and performing a linear regression, ρ_{Ag} (= 1.06 μΩ cm) is obtained. The resistivity of Py, ρ_{Py} (= 22.4 μΩ cm), is measured separately in a device for which Py was grown under the same evaporation conditions. By setting λ_{Py}= 5 nm [36] and α_{Py}= 0.33 [6,7,9] we fit our experimental data to Eq. (1) and we obtain the fitting parameters $\alpha_i = 0.47 \pm 0.04$ and $\lambda_{Ag} = 823 \pm 59$ nm at 10 K for epitaxially grown Ag. For comparison, the control sample with polycrystalline growth yields a higher Ag resistivity, ρ_{Ag} = 2.22 μΩ cm, a lower spin diffusion length, $\lambda_{Ag} = 449 \pm 30$ nm and a lower interface spin polarization $\alpha_i = 0.25 \pm 0.03$ at 10 K. These values are comparable to other polycrystalline Ag samples reported in literature [17,18, 21].

This substantial improvement in the spin diffusion length, by a factor of two, can be related to the decrease of the spin relaxation via grain boundary scattering [7,15]. As it has been previously observed, the polycrystalline sample shows a considerably smaller

grain size in comparison to the epitaxial Ag. The smaller grain size implies having more grain boundaries, and consequently a higher resistivity and a shorter λ_{Ag}. Moreover, grains do not have a preferred crystallographic orientation for the polycrystalline Ag case, so that the existing grain boundaries are high angle grain boundaries, which also contributes to a higher resistivity. In contrast, the epitaxial growth of Ag strongly reduces the grain boundaries in the channel, which lowers the resistivity to $\rho_{Ag} \backsim 1.07$ μΩ cm and increases λ_{Ag}. This dependence is in good agreement with the EY mechanism, which predicts $\lambda_{Ag} \propto \frac{1}{\rho_{Ag}}$ [37]. This mechanism is probably similar to what a thermal annealing might do to polycrystalline Ag. For LSVs where Ag has not been treated, λ_{Ag}~550 nm [17,18] is obtained, whereas values of λ_{Ag}~1000 nm have been reported after thermally treating the devices [15,21]. However, the advantage of controlling the Ag growth by means of epitaxy is that there is no need for additional thermal treatment, and given that the growth is done at room temperature, possible thermal diffusion between metals is avoided.

In conclusion, we have shown that the spin diffusion length in Ag can be substantially increased by controlling the growth process. When epitaxial Ag is grown, the grain boundary scattering is largely suppressed leading to lower resistivity values and higher spin diffusion lengths. The main advantage that this approach offers compared to an annealing treatment is that the growth process is done at room temperature. This avoids a possible diffusion of metals when the device is being heated. Proper engineering of the material used as a spin channel can thus improve the spin transport properties, and hereby help towards the development of devices based on pure spin currents.

Acknowledgments

This work is supported by the European Union 7th Framework Program under the Marie Curie Actions (256470-ITAMOSCINOM) and the European Research Council (257654-SPINTROS), by the Spanish MINECO (MAT2012-37638 and MAT2012-36844) and by the Basque Government (PI2011-1 and PI2012-47). M. I., E. V., L. F. and O. I. thank the Basque Government for a PhD fellowship (BFI-2011-106, BFI-2010-163, PRE-2013-1-974 and BFI-2009-284, respectively).

REFERENCES

[1] B. Behin-Aein, D. Datta, S. Salahuddin, and S. Datta, Nature Nanotech. **5**, 266 (2010).
[2] M. Johnson and R. H. Silsbee, Phys. Rev. Lett. **55**, 1790 (1985).
[3] M. Johnson and R. H. Silsbee, Phys. Rev. B **37**, 5312 (1988).
[4] F. J. Jedema, A. T. Filip and B.J. van Wees, Nature **410**, 345 (2001).
[5] F. J. Jedema, M. S. Nijboer, A. T. Filip and B.J. van Wees, Phys. Rev. B **67**, 085319 (2003).
[6] E. Villamor, M. Isasa, L.E. Hueso and F. Casanova, Phys. Rev. B **88**, 174411 (2013).
[7] E. Villamor, M. Isasa, L.E. Hueso and F. Casanova, Phys. Rev. B **87**, 094417 (2013).

[8] Y. Ji, A. Hoffmann, J. E. Pearson and S. D. Bader, Appl. Phys. Lett. **88**, 052509 (2006).
[9] F. Casanova, A. Sharoni, M. Erekhinsky, and I. K. Schuller, Phys. Rev. B **79**, 184415 (2009).
[10] T. Kimura, Y. Otani and J. Harmle, Phys. Rev. B **73**, 132405 (2006).
[11] X. J. Wang, H. Zou, L. E. Ocola, R. Dican and Y. Ji, Appl. Phys. **105**, 093907 (2009).
[12] M. Erekhinsky, A. Sharoni, F. Casanova, and I. K. Schuller, Appl. Phys. Lett. **96**, 022513 (2010).
[13] S. O. Valenzuela and M. Tinkham, Appl. Phys. Lett. **85**, 24, 5914 (2004).
[14] J. C. Rojas Sánchez, P. Lackowski, W. F. Savero Torres, M. Cubucku, V. D. Nguyen, L. Notin, C. Beigné, C. Vergnaud, M. Jamet, L. Vila and J. P. Attané, Appl. Phys. Lett. **102**, 132408 (2013).
[15] L. Wang, Y. Fukuma, H. Idzuchi, G. Yu, Y. Jiang and Y. Otani, Appl. Phys. Express **4**, 093004 (2011).
[16] T. Kimura and T. Otani, Phys. Rev. Lett. **99**, 196604 (2007).
[17] Y. Fukuma, L. Wang, H. Idzuchi and Y. Otani, Appl. Phys. Lett. **97**, 012507 (2010).
[18] G. Mihajlovic, J. E. Pearson, S. D. Bader and A. Hoffmann, Phys. Rev. Lett. **104**, 237202 (2010).
[19] H. Idzuchi, Y. Fukuma, L. Wang and Y. Otani, Appl. Phys. Lett. **101**, 022415 (2012).
[20] G. Mihajlovic, D. K. Schreiber, Y. Liu, J. E. Pearson, S. D. Bader, A. K. Petford-Long and A. Hoffmann, Appl. Phys. Lett. **97**, 112502 (2010).
[21] Y. Fukuma, L. Wang, H. Idzuchi, S. Takahashi, S. Maekawa and Y. Otani, Nature Mat. **10**, 527 (2011).
[22] R. Godfrey and M. Johnson, Phys. Rev. Lett. **96**, 136601 (2006).
[23] M. Isasa, E. Villamor, L.E. Hueso, M. Gradhand and F. Casanova, Phys. Rev. B **91**, 024402 (2015).
[24] X. Lou, C. Adelmann, S.A. Crooker, E. S. Garrid, J. Zhang, K. S. M. Reddy, S. D. Flexner, C. J. Palmsrom and P. A. Crowell, Nature Phys. **3**, 197 (2007).
[25] O. M. J. van 't Erve, A. T. Hanbicki, M. Holub, C. H. Li, C. Awo-Affouda, P. E. Thompson, and B. T. Jonker, Appl. Phys. Lett. **91**, 212109 (2007).
[26] J. Li and I. Appelbaum, Phys. Rev. B **84**, 165318 (2011).
[27] L. E. Hueso, J. M. Pruneda, V. Ferrari, G. Burnell, J. P. Valdés-Herrera, B. D. Simons, P. B. Littlewood, E. Artacho, A. Fert and N. D. Mathur, Nature. **445**, 410 (2006).
[28] N. Tombros, C. Jozsa, M. Popinciuc, H. T. Jonkman and B. J. van Wees, Nature 448, 571 (2007).
[29] R. J. Elliott, Phys. Rev. **96**, 266 (1954).
[30] Y. Yafet, Solid State Physics, edited by F. Seitz and D. Turnbull (Academic Press, New York, 1963), pp. 1-98.
[31] W. Yang, D. Lambeth and D. E. Laughlin, J. Appl. Phys. **85**, 4723 (1999).
[32] O. Idigoras, A. K. Suszka, P. Vavassori, P. Landeros, J.M. Porro and A. Berger, Phys. Rev. B **84**, 132403 (2011).
[33] O. Idigoras, A. K. Suszka, P. Vavassori, B. Obry, B. Hillebrands, P. Landeros and A. Berger, J. Appl. Phys. **115**, 083912 (2014).

[34] W. Yang and D. N. Lambeth, J. Appl. Phys. 85, 4723 (1999).
[35] S. Takahashi and S. Maekawa, Phys. Rev. B **67**, 052409 (2003).
[36] S. Dubois, L. Piraux, J. M. George, K. Ounadjela, J. L. Duvail and A. Fert, Phys. Rev. B **60**, 477 (1999).
[37] The spin diffusion length is defined as $\sqrt{D\tau_{sf}}$, being $D = 1/N(E_F)\,e^2\rho$ the diffusion constant, $N(E_F)$ the electronic density of states at the Fermi level, e the electronic charge, ρ the resistivity and τ_{sf} the spin relaxation time of the NM metal, Ag in this case. For the particular case of metals, as discussed by EY [28,29], the spin relaxation time is directly proportional to the momentum relaxation time, τ_e, in the form of $\tau_{sf} = \tau_e/a$, where a is the spin flip-probability. τ_e can be calculated from $\tau_e = 3/v_F^2\,N(E_F)e^2\rho$, where v_F is the Fermi velocity. Therefore, the spin diffusion length dependence on the resistivity is expected to be $\lambda_{Ag} \propto \frac{1}{\rho_{Ag}}$.